

Electronic Supplementary Information

Implications of magnetic dilution of PrFeO₃ with Bi³⁺ on its dielectric and magnetic properties

Shivangi Rao,^a Subhajit Sau,^b V. Kanchana,^b G. Vaitheswaran,^{*c} and Rajamani Nagarajan^{*a}

^a Materials Chemistry Group, Department of Chemistry, University of Delhi, Delhi-110007, India.
E-mail: 18darklotus@gmail.com, rnagarajan@chemistry.du.ac.in

^b Department of Physics, Indian Institute of Technology Hyderabad, Kandi - 502285, Sangareddy, Telangana, India. Email: ph21resch01001@iith.ac.in, kanchana@phy.iith.ac.in

^c School of Physics, University of Hyderabad, Prof. C. R. Rao Road, Gachibowli, Hyderabad, 500046, Telangana, India. E-mail: vaithhee@uohyd.ac.in

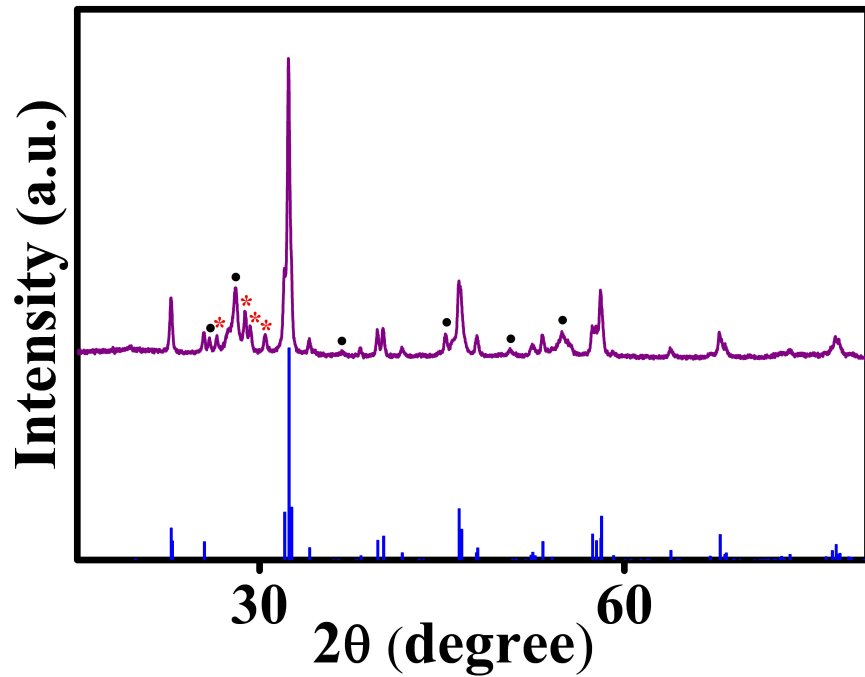


Fig.S1: Line profile of PrFeO₃ (ICSD No: : 98-002-7274) and PXRD pattern of the calcined precursor of Pr_{0.70}Bi_{0.30}FeO₃ at 800 °C for 12 h in the air. The reflections marked with ‘●’ and ‘★’ correspond to tetragonal Bi₂O_{2.5} (ICSD No: 98-001-0470), and hexagonal Pr₂O₃ (ICSD No: 98-006-1179), respectively.

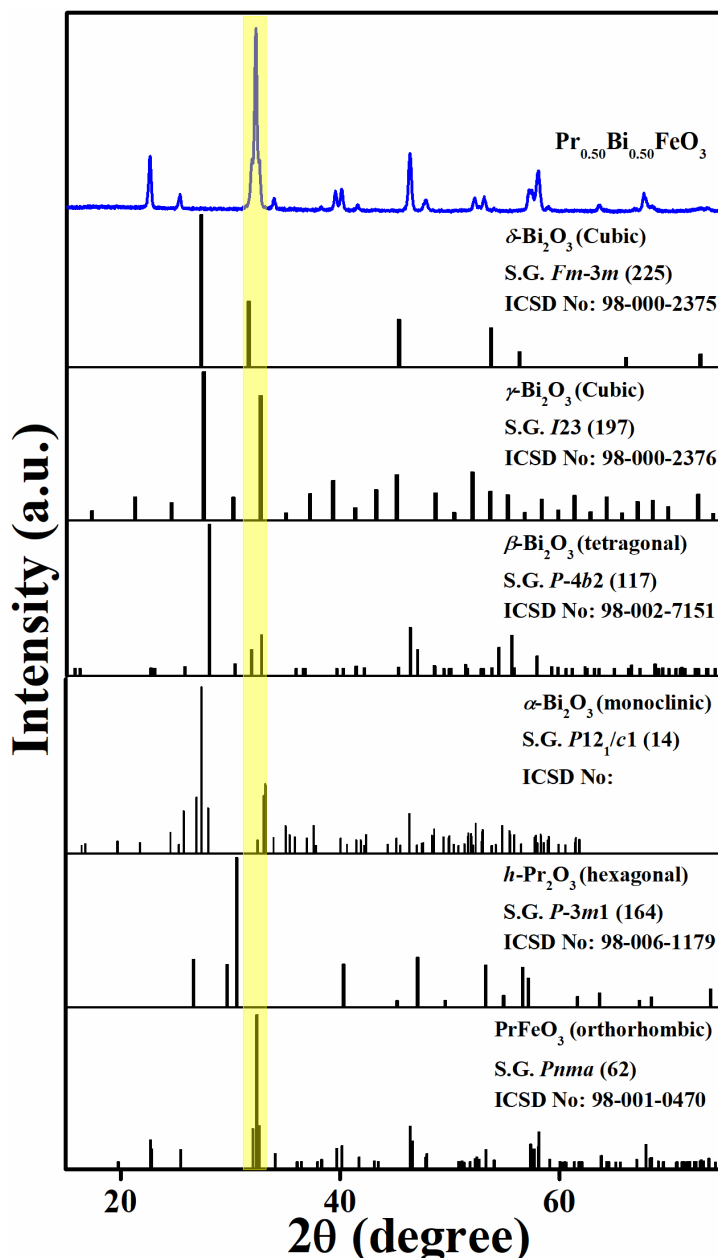


Fig.S2: Comparison of line profiles of PrFeO₃ and possible secondary phases, including Pr₂O₃ and various polymorphs of Bi₂O₃ with the PXRD pattern of Pr_{0.50}Bi_{0.50}FeO₃ sample prepared under flowing argon atmosphere.

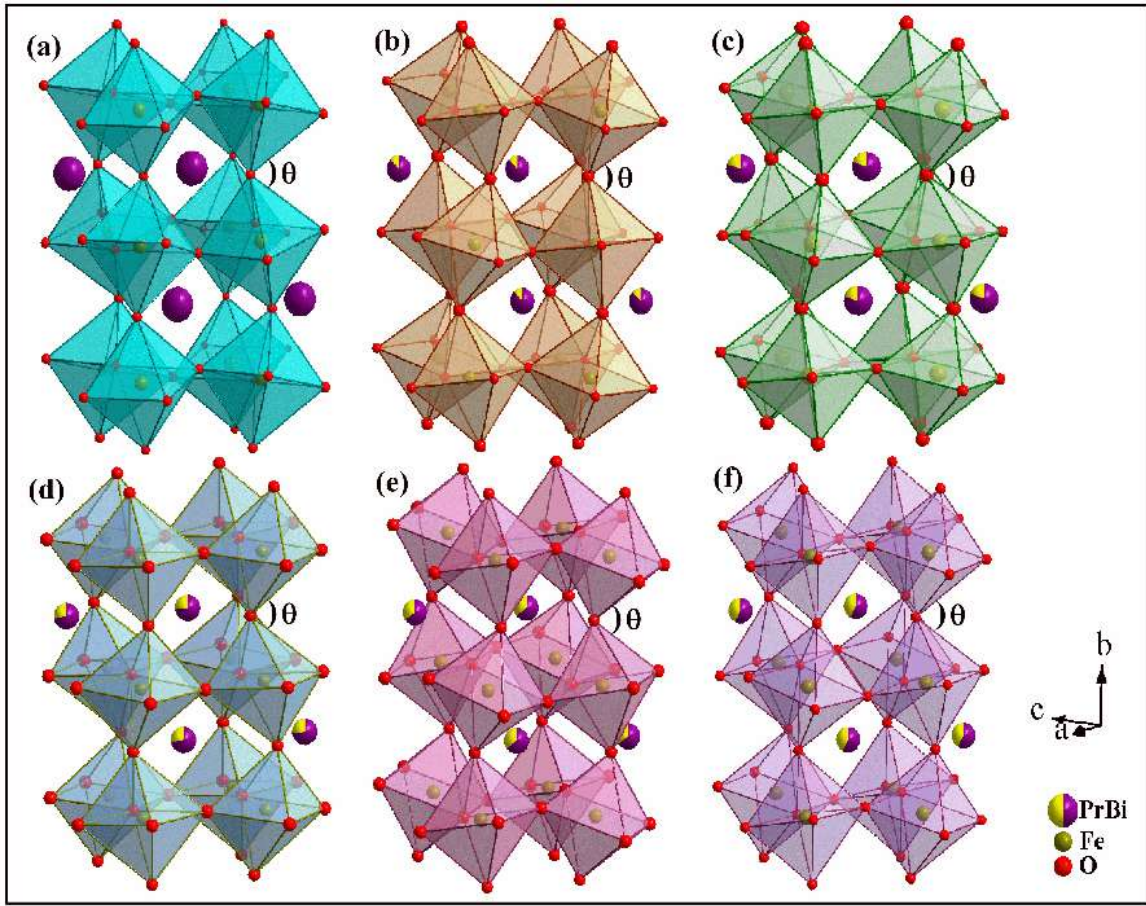


Fig.S3: Octahedral tilting occurring in the orthorhombically distorted perovskite structure of $\text{Pr}_{1-x}\text{Bi}_x\text{FeO}_3$ with x , (a) 0.00, (b) 0.10, (c) 0.20, (d) 0.30, (e) 0.40, and (f) 0.50.

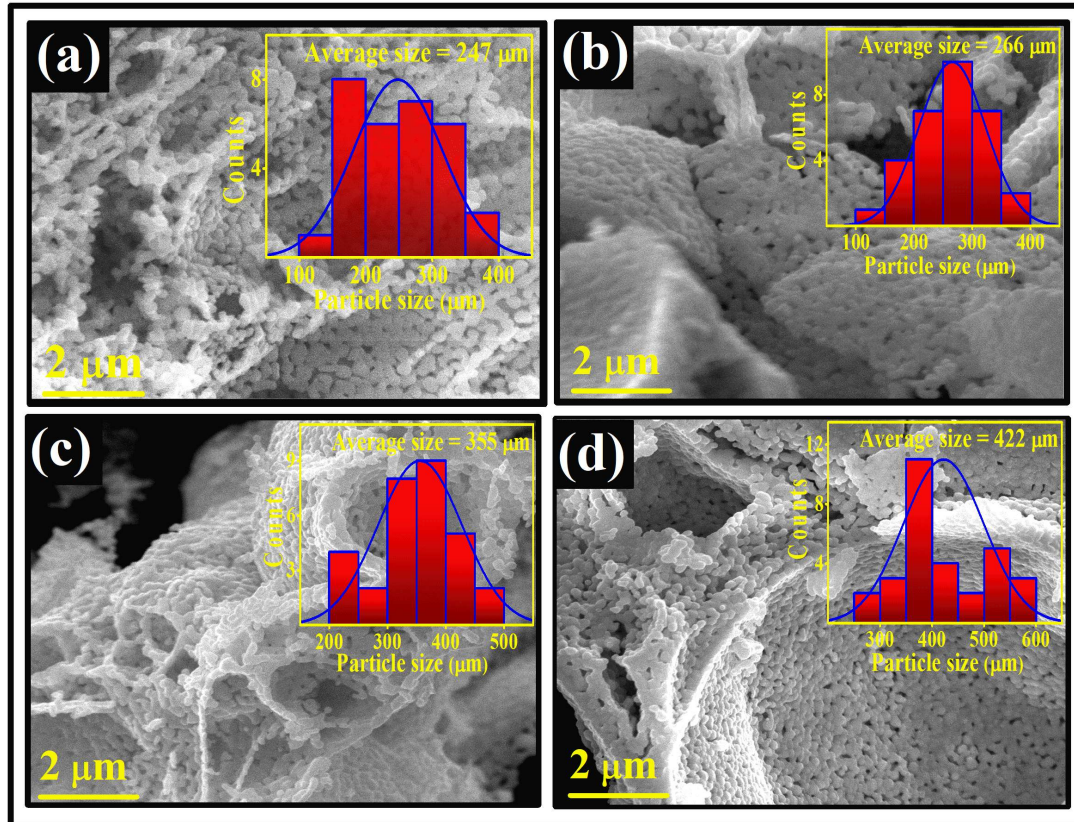


Fig.S4: SEM images and particle size distribution of $\text{Pr}_{1-x}\text{Bi}_x\text{FeO}_3$ samples with x being (a) 0.10, (b) 0.20, (c) 0.40, and (d) 0.50.

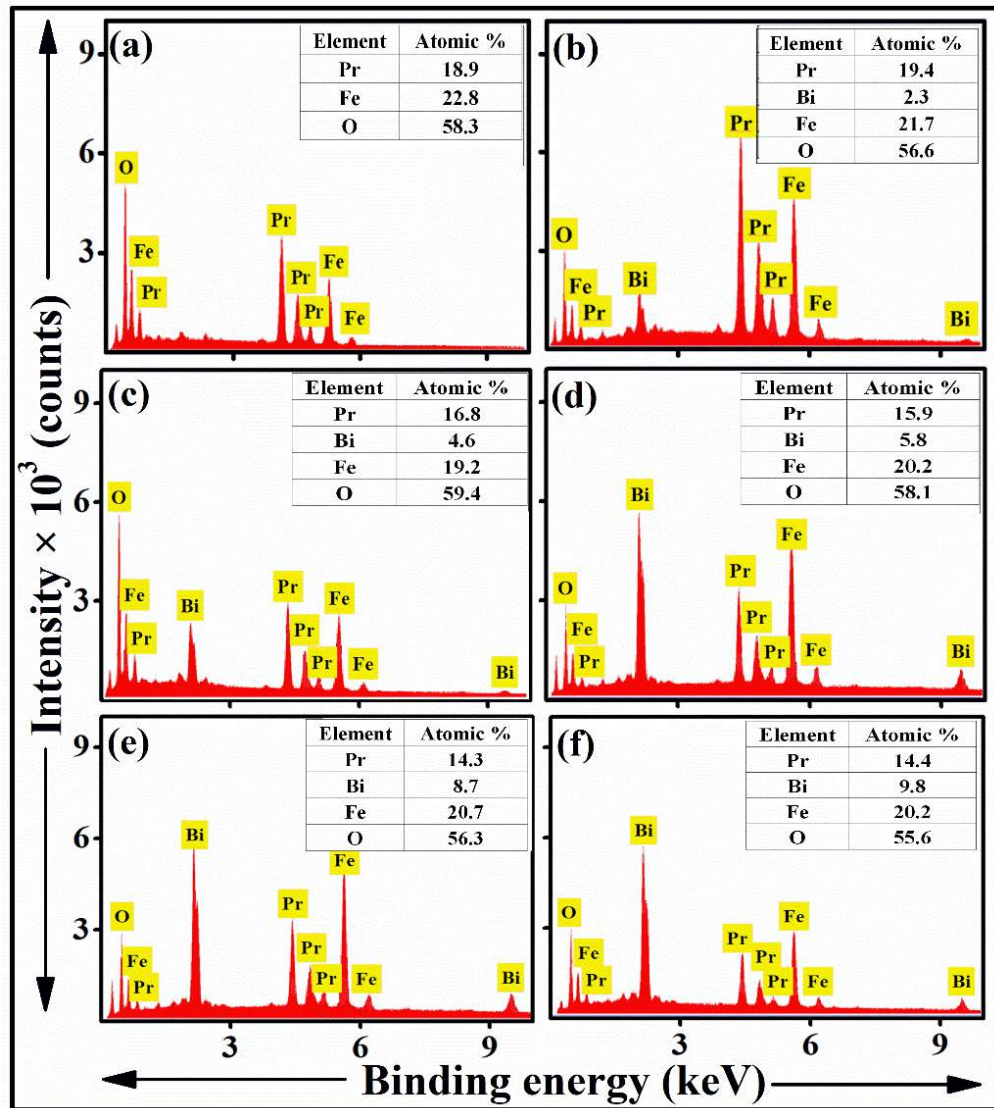


Fig.S5: EDS spectrum of $\text{Pr}_{1-x}\text{Bi}_x\text{FeO}_3$ samples with x being 0.00 (a), 0.10 (b), 0.20 (c), 0.30 (d), 0.40 (e), and 0.50 (f).

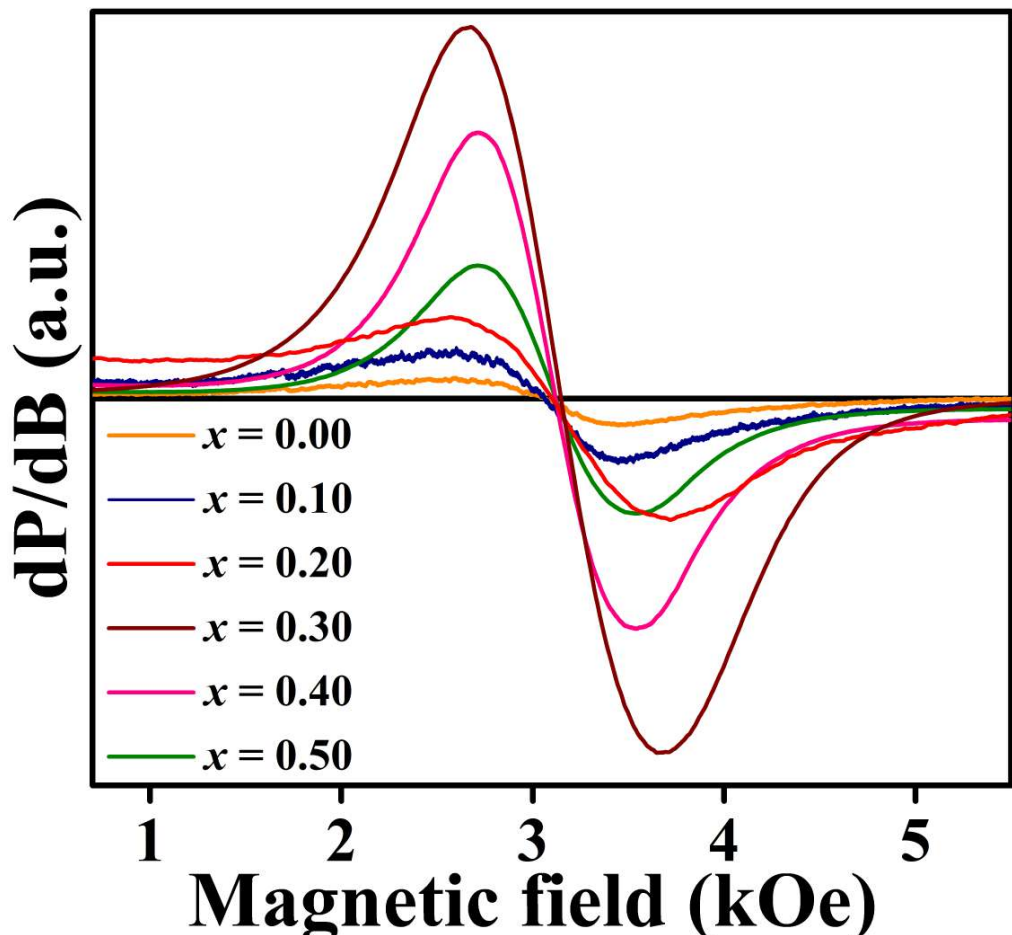


Fig.S6: Room temperature EPR spectra of $\text{Pr}_{1-x}\text{Bi}_x\text{FeO}_3$ samples.

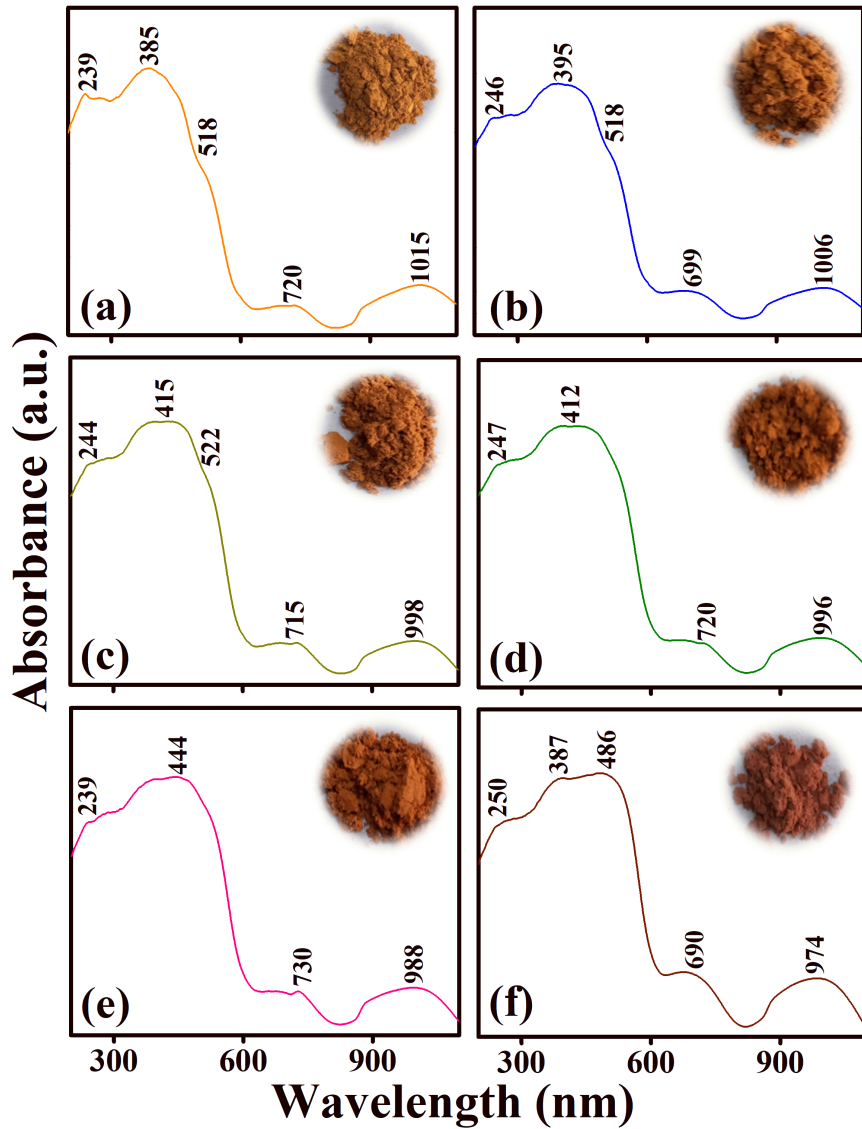


Fig.S7: UV-Visible absorbance spectra of $\text{Pr}_{1-x}\text{Bi}_x\text{FeO}_3$ (a) 0.00, (b) 0.10, (c) 0.20, (d) 0.30, (e) 0.40 and (f) 0.50. The digital images of the samples are shown as insets.

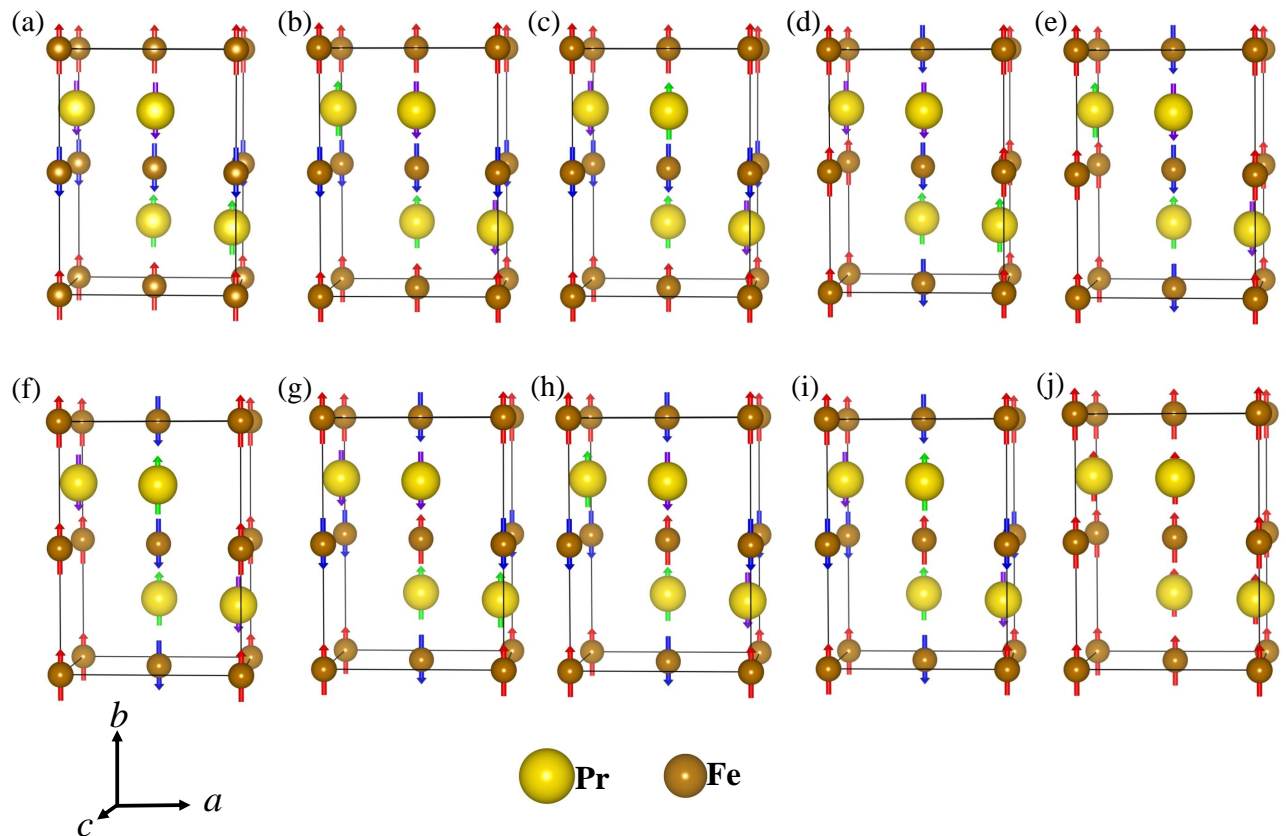


Fig.S8: Magnetic configuration in (a) Fe with A-AFM and Pr with A-AFM like arrangement. (b) Fe with A-AFM and Pr with C-AFM like arrangement. (c) Fe with A-AFM and Pr with G-AFM like arrangement. Similarly, for (d-f) spin arrangement of Pr was varied in A-, C-, and G- like configurations with fixed Fe C-AFM. (g-i) spin arrangement of Pr was varied in A-, C-, and G- like configurations with fixed Fe with G-AFM, and (j) FM configurations of pristine PrFeO_3 considered in the present work (O atoms not shown in the figures). (h) is the ground state configuration.

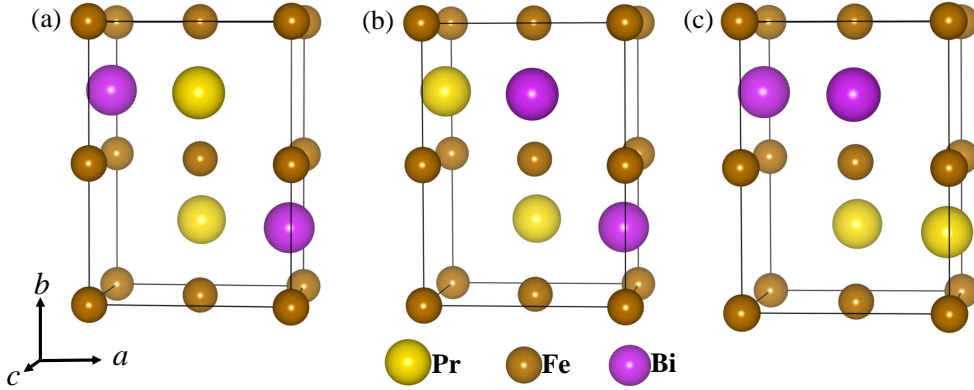


Fig.S9: (a-c) Three possible combinatorial configurations with 50% Bi substituted PrFeO_3 . The energy was calculated in $\text{Pr}(\text{up})-\text{Pr}(\text{up})$, $\text{Pr}(\text{up})-\text{Pr}(\text{dn})$, and $\text{Pr}(\text{dn})-\text{Pr}(\text{dn})$ spin for each structure with Fe atoms' G-AFM configuration (A- and C-AFM spin arrangement of Fe not considered here). Among these three structures, (b) is the ground state with both Pr up spin and Fe with G-AFM configuration.

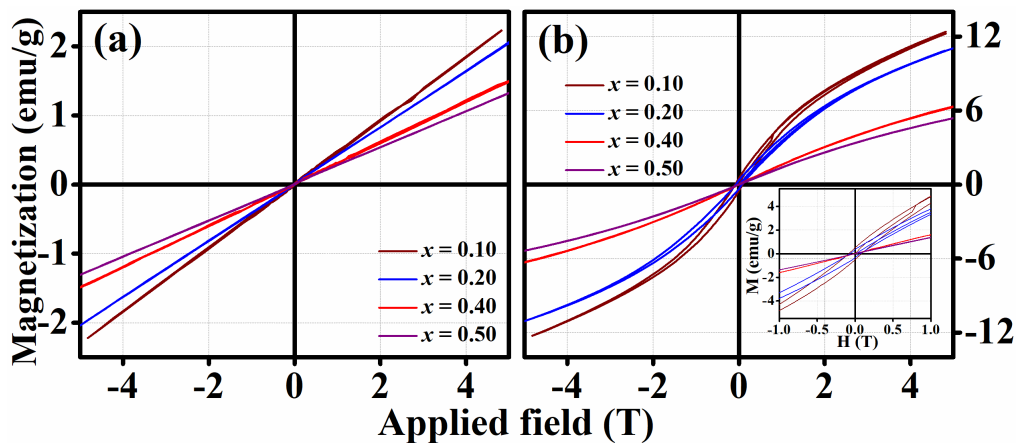


Fig.S10: (a) and (b) Plots of magnetization vs. magnetic field of $\text{Pr}_{1-x}\text{Bi}_x\text{FeO}_3$ samples, x being 0.10, 0.20, 0.40, and 0.50 at 298 and 2 K, respectively.

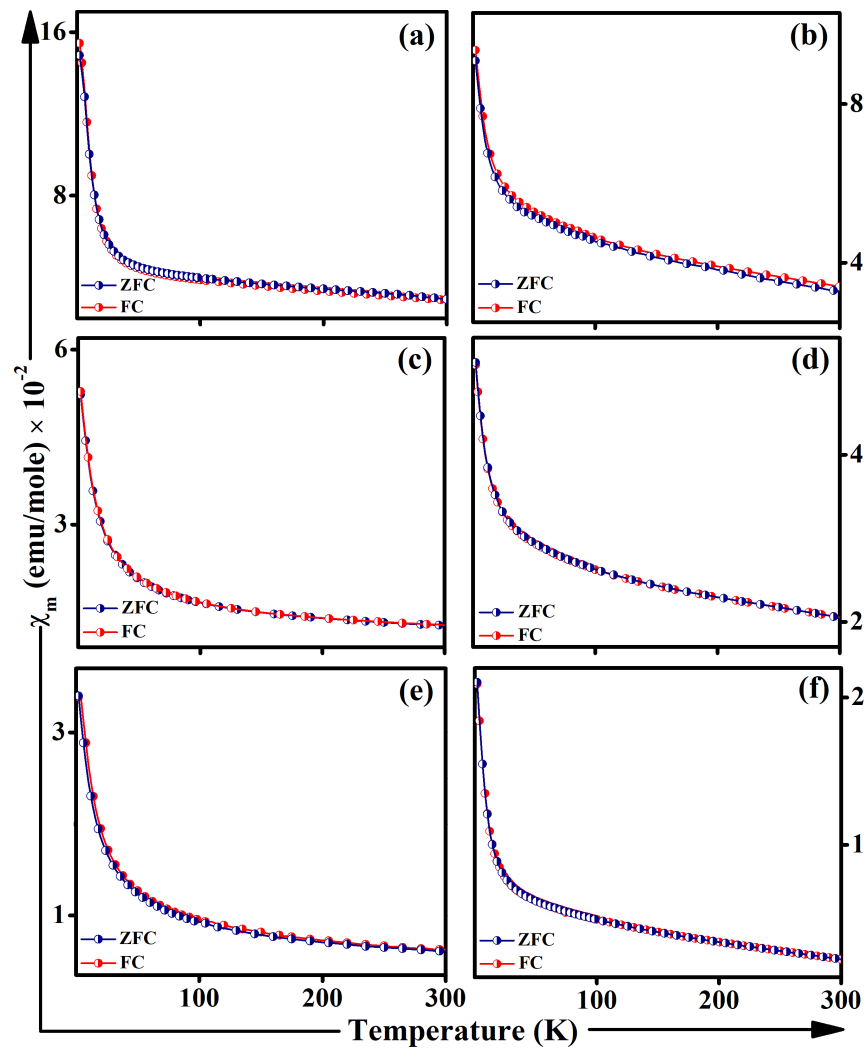


Fig.S11: Temperature dependence of molar magnetic susceptibility of $\text{Pr}_{1-x}\text{Bi}_x\text{FeO}_3$ samples x being 0.00 (a), 0.10 (b), 0.20 (c), 0.30 (d), 0.40 (e) and 0.50 (f) measured under ZFC (data in blue) and FC (data in red) conditions at 0.1 T.

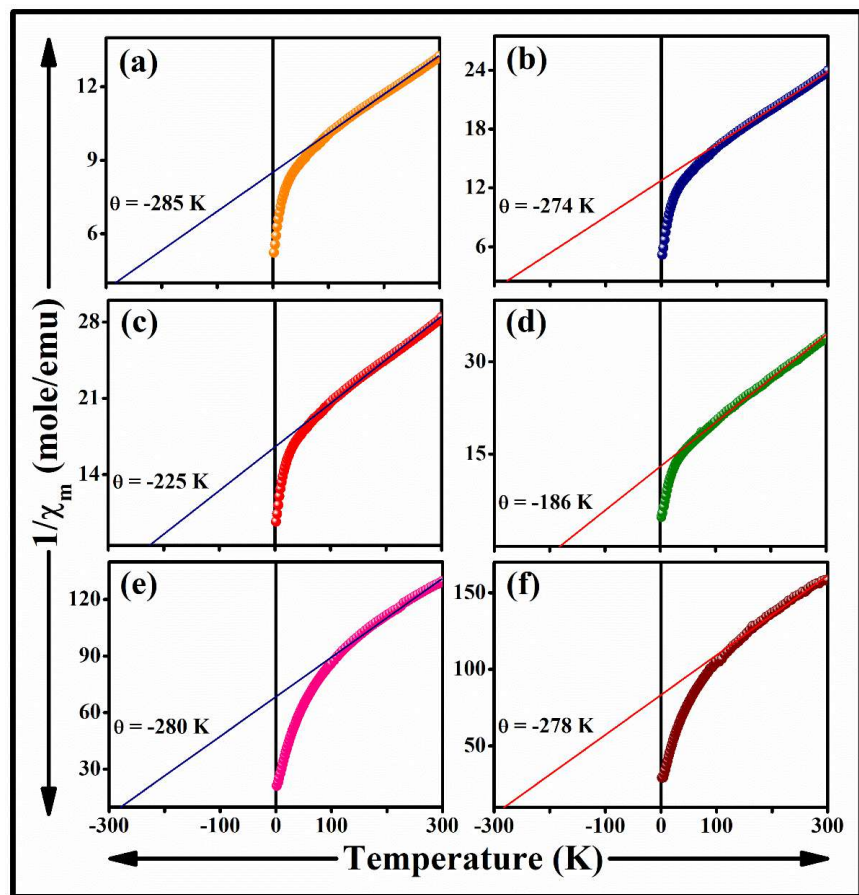


Fig.S12: Plots of the temperature dependence of inverse molar susceptibility ($1/\chi_m$ vs. T) of $\text{Pr}_{1-x}\text{Bi}_x\text{FeO}_3$ samples with x being (a) 0.00, (b) 0.10, (c) 0.20, (d) 0.30, (e) 0.40 and (f) 0.50 (data in wine), considering the field cooled (FC) curves measured at $H = 0.1$ T and fitted with Curie–Weiss law in the temperature range of 150 to 300 K.

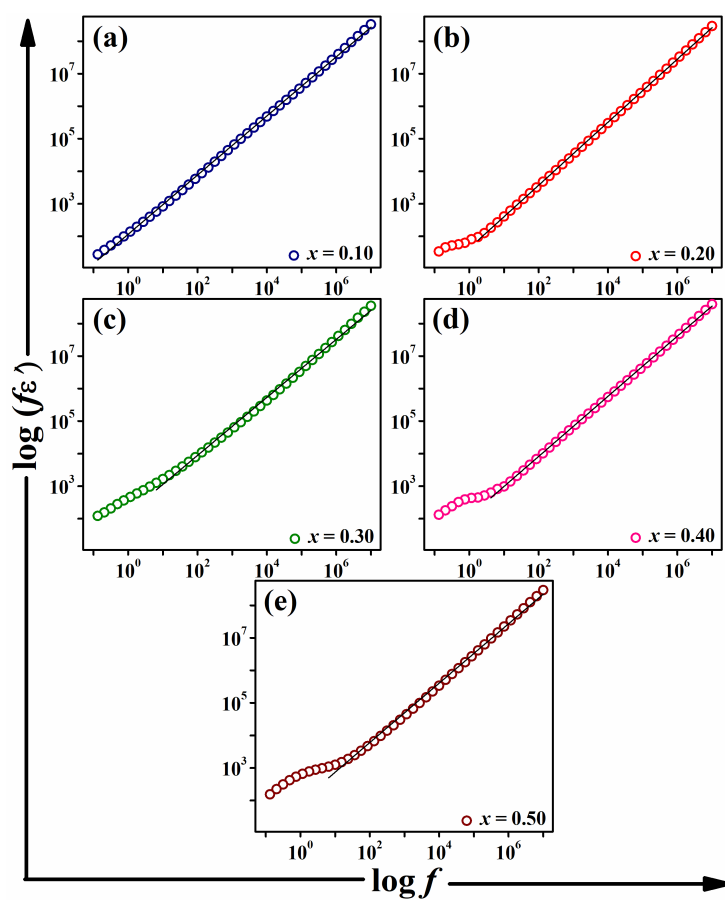


Fig.S13: (a-e) Plot of $\log(f\varepsilon')$ vs $\log f$ of the $\text{Pr}_{1-x}\text{Bi}_x\text{FeO}_3$ samples ($x = 0.10-0.50$).

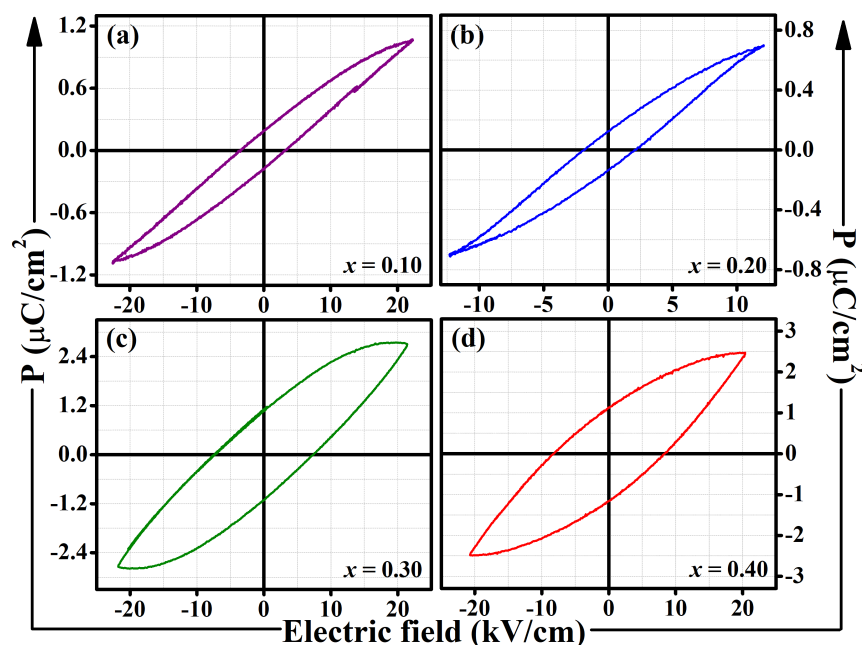


Fig.S 14: Ferroelectric-hysteresis loops of (a) $\text{Pr}_{0.90}\text{Bi}_{0.10}\text{FeO}_3$, (b) $\text{Pr}_{0.80}\text{Bi}_{0.20}\text{FeO}_3$, (c) $\text{Pr}_{0.70}\text{Bi}_{0.30}\text{FeO}_3$ and (d) $\text{Pr}_{0.60}\text{Bi}_{0.40}\text{FeO}_3$ samples.

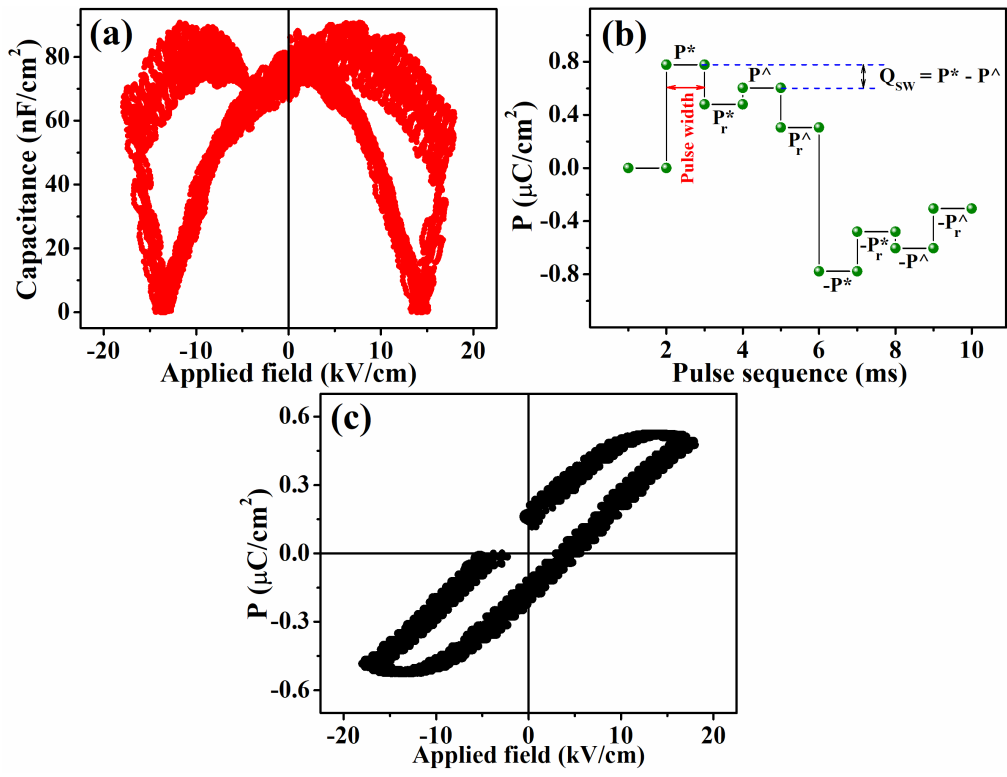


Fig.S15: (a) C-V plot, (b) PUND characteristics at an applied field of 20 kV and pulse width 1 ms, and (c) P-E loop after PUND analysis for $\text{Pr}_{0.60}\text{Bi}_{0.40}\text{FeO}_3$ sample.

Table S1: Details of the amounts of reactants used to synthesize Bi-substituted PrFeO_3 samples.

S. No	Composition	Pr_2O_3 , g (mmol)	Bi_2O_3 , g (mmol)	Fe metal powder, g (mmol)	CA, g (mmol)
1	PrFeO_3	0.1649 (0.50)	—	0.0558 (1.00)	0.3458 (1.80)
2	$\text{Pr}_{0.90}\text{Bi}_{0.10}\text{FeO}_3$	0.1484 (0.45)	0.0232 (0.05)	0.0058 (1.00)	0.3458 (1.80)
3	$\text{Pr}_{0.80}\text{Bi}_{0.20}\text{FeO}_3$	0.1319 (0.40)	0.0466 (0.10)	0.0058 (1.00)	0.3458 (1.80)
4	$\text{Pr}_{0.70}\text{Bi}_{0.30}\text{FeO}_3$	0.1154 (0.35)	0.0698 (0.15)	0.0058 (1.00)	0.03458 (1.80)
5	$\text{Pr}_{0.60}\text{Bi}_{0.40}\text{FeO}_3$	0.0989 (0.30)	0.0931 (0.20)	0.0058 (1.00)	0.3458 (1.80)
6	$\text{Pr}_{0.50}\text{Bi}_{0.50}\text{FeO}_3$	0.0822 (0.25)	0.1165 (0.25)	0.0058 (1.00)	0.3458 (1.80)

Table S2: Atomic parameters from the final refinement cycle of the PXRD patterns for $\text{Pr}_{1-x}\text{Bi}_x\text{FeO}_3$ samples ($x = 0.00, 0.10, 0.20, 0.30, 0.40$, and 0.50) by the Rietveld method.

Composition (x)	Atoms	Wyck	x/a	y/b	z/c	SOF	$\mathbf{U}(\text{iso}) \text{ \AA}^2$
0.00	Pr	$4c$	0.4569(2)	0.25	0.0092(5)	1.0	0.022(4)
	Fe	$4a$	0	0	0	1.0	0.017(8)
	O1	$8d$	0.2072(2)	0.0347(1)	0.2879(2)	1.0	0.023(3)
	O2	$4c$	0.5183(2)	0.25	0.5827(3)	1.0	0.027(4)
0.10	Pr	$4c$	0.4567(2)	0.25	0.0094(5)	0.88(9)	0.023(4)
	Bi	$4c$	0.4567(2)	0.25	0.0094(5)	0.12(9)	0.023(4)
	Fe	$4a$	0	0	0	1.0	0.018(1)
	O1	$8d$	0.2121(2)	0.0330(2)	0.2894(2)	1.0	0.016(3)
	O2	$4c$	0.5188(2)	0.25	0.5758(2)	1.0	0.027(5)
0.20	Pr	$4c$	0.4565(2)	0.25	0.0089(5)	0.79(2)	0.03(7)
	Bi	$4c$	0.4565(2)	0.25	0.0089(5)	0.21(2)	0.03(7)
	Fe	$4a$	0	0	0	1.0	0.028(1)
	O1	$8d$	0.2057(2)	0.0293(2)	0.2934(3)	1.0	0.021(4)
	O2	$4c$	0.5235(3)	0.25	0.577(4)	1.0	0.034(8)
0.30	Pr	$4c$	0.4566(1)	0.25	0.0093(5)	0.74(2)	0.023(2)
	Bi	$4c$	0.4566(1)	0.25	0.0093(5)	0.26(2)	0.023(2)
	Fe	$4a$	0	0	0	1.0	0.020(5)
	O1	$8d$	0.2027(3)	0.0292(3)	0.2816(4)	1.0	0.028(4)
	O2	$4c$	0.5221(4)	0.25	0.567(4)	1.0	0.025(3)
0.40	Pr	$4c$	0.4565(2)	0.25	0.0088(2)	0.63(5)	0.024(6)
	Bi	$4c$	0.4565(2)	0.25	0.0088(2)	0.37(5)	0.024(6)
	Fe	$4a$	0	0	0	1.0	0.021(4)
	O1	$8d$	0.2096(1)	0.0292(2)	0.2887(4)	1.0	0.024(3)
	O2	$4c$	0.5181(3)	0.25	0.5668(2)	1.0	0.027(5)
0.50	Pr	$4c$	0.4566(1)	0.25	0.009(3)	0.58(7)	0.023(2)
	Bi	$4c$	0.4566(1)	0.25	0.009(3)	0.42(7)	0.023(2)
	Fe	$4a$	0	0	0	1.0	0.017(5)
	O1	$8d$	0.2151(2)	0.0378(1)	0.2758(2)	1.0	0.019(2)
	O2	$4c$	0.5173(1)	0.25	0.5646(2)	1.0	0.02(3)

Table S3: Lattice parameters and selected bond distances and angles of the $\text{Pr}_{1-x}\text{Bi}_x\text{FeO}_3$ samples ($x = 0.00, 0.10, 0.20, 0.30, 0.40$, and 0.50) from the final refinement cycle of the PXRD patterns by the Rietveld method.

Composition (x)	0.00	0.10	0.20	0.30	0.40	0.50
a (\AA)	5.5774(7)	5.5785(4)	5.5853(7)	5.5943(2)	5.6089(1)	5.6104(1)
b (\AA)	7.7908(1)	7.7922(2)	7.797(1)	7.7995(3)	7.8371(2)	7.8385(2)
c (\AA)	5.4848(7)	5.4862(2)	5.4874(8)	5.4875(2)	5.4941(2)	5.4972(1)
Cell Volume (\AA^3)	238.32(6)	238.48(8)	238.82(5)	240.11(7)	241.51(5)	241.8(6)
Fe–O1 ($\times 2$)	1.9939(5)	1.9943(4)	1.9950(7)	1.9978(2)	1.9989(2)	2.0005(2)
Fe–O1 ($\times 2$)	1.9960(4)	1.9968(4)	1.9983(7)	1.9991(2)	2.0005(3)	2.0011(2)
Fe–O2 ($\times 2$)	1.9898(3)	1.9936(5)	1.9945(7)	1.9972(3)	1.9991(3)	2.0002(2)
Fe–O	1.9932	1.9949	1.9959	1.9980	1.9995	2.0006
Fe–O1–Fe	155.11(2)	155.35(5)	156.20(2)	157.51(7)	158.88(3)	160.59(6)
Fe–O2–Fe	153.76(5)	154.58(6)	155.17(2)	157.14(2)	157.81(4)	158.08(4)
$\theta = \text{Fe–O–Fe} $	154.44	154.97	155.68	157.32	158.34	159.33
$\phi =$ ($180^\circ - \angle\text{Fe–O–Fe} /2$)	12.78	12.52	12.16	11.34	10.82	10.34

Table S4: Summary of magnetic properties of pristine and $\text{Pr}_{1-x}\text{Bi}_x\text{FeO}_3$ samples.

Composition	H_c (T)		M_r (emu/g)		Std. error at 298K (emu)
	at 2 K	at 298 K	at 2 K	at 298 K	
PrFeO_3	0.067	0.200	0.900	0.120	1.77×10^{-5}
$\text{Pr}_{0.90}\text{Bi}_{0.10}\text{FeO}_3$	0.083	0.003	0.500	0.016	1.81×10^{-5}
$\text{Pr}_{0.80}\text{Bi}_{0.20}\text{FeO}_3$	0.071	0.018	0.300	0.0117	2.09×10^{-5}
$\text{Pr}_{0.70}\text{Bi}_{0.30}\text{FeO}_3$	0.065	-	0.200	-	1.72×10^{-5}
$\text{Pr}_{0.60}\text{Bi}_{0.40}\text{FeO}_3$	0.011	-	0.013	-	2.15×10^{-5}
$\text{Pr}_{0.50}\text{Bi}_{0.50}\text{FeO}_3$	0.002	-	0.010	-	1.93×10^{-5}